Advances in Geo-Energy Research

Vol. 5, No. 4, p. 407-421, 2021

Original article

Effect of alcohol-treated CO_2 on interfacial tension between CO_2 and oil, and oil swelling

Saira, Hang Yin, Furqan Le-Hussain*

School of Mineral and Energy Resources, University of New South Wales, Sydney, NSW 2052, Australia

Keywords:
Alcohol-treated CO_2
interfacial tension
miscibility enhancement
oil swelling

Cited as:
Saira, Yin, H., Le-Hussain, F. Effect of alcohol-treated CO_2 on interfacial tension between CO_2 and oil, and oil swelling. Advances in Geo-Energy Research, 2021, 5(4): 407-421, doi: 10.46690/ager.2021.04.06

Abstract:
This paper investigates the extent to which alcohol-treated carbon dioxide (CO_2), a mixture of alcohol and CO_2 equilibrated at experimental pressure and temperature, can lead to greater interfacial tension reduction and greater oil swelling than can pure CO_2. Experimental measurements of interfacial tension and swelling behavior are made using a high-pressure, high-temperature visual cell at 70 °C. Two sets of fluid pairs are used: pure CO_2 and oil, and alcohol-treated CO_2 and oil. Two types of oil are used: a mixture of 35% hexane and 65% decane (C_6-C_{10} mixture), and pure decane (pure C_{10}). Ethanol and methanol are used to prepare alcohol-treated CO_2. Numerical simulations are used to estimate a reduction in the minimum miscibility pressure when using alcohol-treated CO_2. Interfacial tension between alcohol-treated CO_2 and oil is found to be 0.02 to 2.2 mN/m less than that between pure CO_2 and oil. Simulation results suggest that alcohol-treated CO_2 yields 0.2 to 1.2 MPa lower minimum miscibility pressure compared to pure CO_2. Alcohol-treated CO_2 also is found to cause 6% to 43% more swelling of oil than does pure CO_2. Interfacial tension and swelling results suggest that alcohol-treated CO_2 yields better miscibility with oil compared to pure CO_2.

1. Introduction

Carbon capture, utilization, and storage (CCUS) could potentially reduce global warming (Liu et al., 2018; Zhang et al., 2019; Ershadnia et al., 2020; Ren et al., 2021). Among CCUS technologies, carbon dioxide (CO_2) injection into oil reservoirs, also known as CO_2-enhanced oil recovery (CO_2-EOR), is the most economically viable technique (Zhang et al., 2020b; Iglauer and Al-Yaseri, 2021). However, the effectiveness of a CO_2-EOR project is conditional on miscibility (Choubineh et al., 2019; Dong et al., 2019).

Under full miscibility, interfacial tension (IFT) between CO_2 and oil is zero, which means that the injected CO_2 and oil mix to form a single phase. To achieve full miscibility, reservoir pressure needs to be at or above minimum miscibility pressure (MMP) (Dai et al., 2014; Amooie et al., 2017). If reservoir pressure is such that IFT is greater than zero but less than 1 mN/m, then CO_2-EOR is considered near-miscible (Thomas et al., 1994). However, if reservoir pressure is such that IFT is at least 1 mN/m, then CO_2-EOR is considered immiscible (Bedrikovetsky, 2003). Fully miscible and near-miscible CO_2-EOR leads to high oil recovery and CO_2 storage (Ahmed, 2000; Orr, 2007; Amooie et al., 2017), whereas immiscible CO_2-EOR leads to low oil recovery and CO_2 storage (Bagci, 2007; Saira et al., 2021). Therefore, modied CO_2 injection has been employed to enhance miscibility in depleted oil reservoirs (Moradi et al., 2014; Rommerskirchen et al., 2016; Luo et al., 2018; Rommerskirchen et al., 2018; Shang et al., 2018; Yang et al., 2019).

Modifying CO_2 helps to enhance the interaction between CO_2 and oil, thereby reducing IFT and MMP (Saira et al., 2020). Additives used to modify CO_2-oil systems have included alcohols (Moradi et al., 2014; Luo et al., 2018; Shang et al., 2018; Yang et al., 2019), polymers (Gu et al., 2013; Al Hinai et al., 2019), surfactants (Aji et al., 2016; Luo et al., 2018; Kuang et al., 2021), and other chemicals (Rommerskirchen et al., 2016; Rommerskirchen et al., 2018).

Moradi et al. (2014) and Yang et al. (2019) added alcohol in oil to modify a CO_2-oil system. Using the pendant drop technique, which utilizes a high-pressure high-temperature (HPHT) optical cell, they found that the IFT between CO_2 and alcohol-treated oil was 0.3-2.2 mN/m less than the IFT

*Corresponding author.
E-mail address: saira@unsw.edu.au (Saira); hang.yin1@student.unsw.edu.au (H. Yin); furqan.hussain@unsw.edu.au (F. Le-Hussain).

2207-9963
Received October 7, 20201; revised October 27, 2021; accepted October 28, 2021; available online October 29, 2021.

Yandy Scientific Press

between CO_2 and untreated oil. Moradi et al. (2014) used a mixture of alcohol and heptane in oil to modify a CO_2-oil system. They studied linear, branch, and mixed alcohols at various concentrations in order to observe how additive type and concentration affected the IFT between CO_2 and oil. They found that IFT was lower with alcohol-treated oil than with untreated oil, although the difference varied according to additive type and concentration. The overall reduction in IFT achieved by alcohol-treated oil was 0.9-3.2 mN/m. Yang et al. (2019) prepared a mixture of butanol, pentanol, and hexanol in an 8:1:1 proportion by volume and injected it in oil until the alcohols constituted 5% of the overall volume. This was found to produce a lower IFT than did untreated oil. They reported that IFT between CO_2 and untreated oil was 4-26.5 mN/m, whereas IFT between CO_2 and alcohol-treated oil was 2.2-22.5 mN/m. They also plotted the measured IFT values against pressure. They extrapolated IFT versus pressure graph until IFT becomes zero. They suggested that the pressure at which IFT becomes zero is MMP. This graphical approach to estimating MMP is called vanishing interfacial technique (VIT) (Rao, 1997; Ayirala et al., 2003; Ahmad et al., 2016; Almobarak et al., 2021). Yang et al. (2019) further observed a 9.4 MPa reduction in MMP when alcohol-treated oil was used. However, these studies introduced additives directly into oil, which is infeasible in a real reservoir because a reservoir does not permit additives and oil to be uniformly mixed.

Gu et al. (2013), Luo et al. (2018), Rommerskirchen et al. (2018), Shang et al. (2018) and AlHinai et al. (2019) mixed additives into CO_2 to attain full miscibility and used the pendant drop technique to determine IFT values directly and VIT to measure MMP indirectly. Gu et al. (2013) used a mixture of polymers and CO_2, which they equilibrated in an HPHT cylinder. They reported an IFT reduction of 0.7-3.6 mN/m and an MMP reduction of 7.4-7.6 MPa. Al Hinai et al. (2019) used polymers placed on metal plate inside HPHT cell to modify CO_2. They reported slight reduction in IFT with modified CO_2 at lower pressures while 0.5-1.5 mN/m reduction in IFT at high pressures resulted in 5-5.3 MPa reduction in MMP. Shang et al. (2018) soaked a cotton ball in ethanol and passed CO_2 through it. They reported an IFT reduction of 0.5-1.2 mN/m when using 4 wt.% of ethanol in CO_2. Luo et al. (2018) added ethanol or non-ionic surfactant to CO_2. They observed that a greater IFT reduction could be achieved using a smaller concentration of surfactant than of ethanol. They reported an IFT reduction of 1.1-4.7 mN/m with surfactant and 0.73-2.2 mN/m with ethanol. Kuang et al. (2021) used surfactant and mixture of surfactant and alcohol to modify CO_2. They determined IFT values experimentally by using pendant drop technique and MMP by using slim tube experiments. They observed mixture of surfactant and alcohol cause more reduction in IFT as compared to surfactant. They reported 5 MPa reduction in MMP with modified CO_2.

All of the above-mentioned studies used the pendant drop technique to determine IFT values directly. However, these studies examined IFT values only under immiscibility. Therefore, we adopted the capillary rise method suggested by Ayirala and Rao (2006), Sequeira et al. (2008), and Saini and Rao (2010) to directly measure IFT under near-miscibility, which avoids the need to extrapolate an IFT curve. Another limitation is that with the exception of one study (Rommerskirchen et al., 2018), previous work did not measure oil swelling. Oil swelling can lead to improved displacement of oil, due to CO_2 solubility (Lake, 1989). Oil swelling causes the expanded oil to be pushed out of the pore space toward a production well (Tunio et al., 2011; Chen et al., 2021).

Rommerskirchen et al. (2018) studied swelling behavior of modified CO_2, but the additive used in their study is confidential. In this paper, we report the swelling factor in order to further delineate the mechanism of alcohol-treated CO_2 injection. Furthermore, previous alcohol-treated CO_2 studies were limited to high IFT values (>1 mN/m) and swelling factor was not measured. To address these gaps, experiments are performed to assess the extent to which alcohol-treated CO_2 can reduce IFT, enhance miscibility, and increase the oil swelling factor.

2. Materials and methods

We used alcohols to modify CO_2. Other types of additives, polymers, and surfactants are generally less desirable additives because of their low solubility below cloud points (Gupta and Shim, 2006; Li et al., 2019), loss of additive due to adsorption on rock surfaces (Kathel and Mohanty, 2013; Bikkina et al., 2016), and toxicity (Renner, 2004; Li et al., 2019).

2.1 Fluids

For the oil phase, we used (i) a mixture of 0.65 hexane (C_6) and 0.35 decane (C_{10}) by molar fraction (C_6-C_{10} mixture), and (ii) pure decane (pure C_{10}). For the gas phase, we used pure CO_2 and alcohol-treated CO_2, where the alcohol was methanol or ethanol. Studies have shown that heavier alcohol can reduce IFT between CO_2 and oil more than does lighter alcohol (Moradi et al., 2014; Yang et al., 2019). However, we selected methanol and ethanol because they are more soluble in CO_2 than are heavier alcohols, as recommended by Chen et al. (2002), Chen et al. (2003), and Joung et al. (2001). Moradi et al. (2014) and Yang et al. (2019) were able to use heavy alcohol only because it was mixed with oil rather than CO_2. The purities and suppliers of materials used in this study are presented in Table 1.

Alcohol-treated CO_2 was prepared by equilibrating CO_2 with alcohol in an accumulator at experimental temperature and pressure. First, alcohol was placed in the accumulator. Then pure CO_2 was injected to pressurize the accumulator, and temperature was increased using electric heating tape. After the desired pressure and temperature were reached, these conditions were sustained for two hours so that the mixture would reach vapor-liquid equilibrium (Bezanehtak et al., 2002; Tsivintzelis et al., 2004). The composition of alcohol-treated CO_2 was determined using flash calculations performed by CMG-WinProp (2018) software. Table 2 presents fluid properties at experimental conditions and respective molar fractions of alcohol in CO_2. These properties were obtained using the Peng-Robinson equation of state (CMG-WinProp, 2018). Molar fractions of alcohol in CO_2 were determined to closely agree with experimental data reported by Li et al. (2005). Pure

Table 1. Purities and suppliers of used materials.

Chemical	Supplier	Product number	Purity(%)
CO_2	Core Gas Pty Ltd	UN1013	99.5
n-Hexane	Chem-Supply Pty Ltd Australia	HA017-2.5L-P	95.0
n-Decane	Aldrich	30570-1L	95.0
Methanol	Chem-Supply Pty Ltd Australia	MA004-2.5L-J	99.9
Ethanol	Chem-Supply Pty Ltd Australia	EA043-2.5L-J	99.5

Table 2. Injection fluid properties at experimental conditions.

Injection fluid	Pressure (MPa)	Molar fraction of alcohol (%)	Density (kg/m^3)	Viscosity (mPa·s)
CO_2	7.6	0	164	0.020
	8.96	0	211	0.022
	10.34	0	266	0.025
	11.1	0	296	0.026
Methanol-treated CO_2	7.6	3.76	173	0.021
	8.96	4.0	231	0.023
	9.7	4.0	265	0.025
	10.7	4.0	325	0.028
Ethanol-treated CO_2	7.6	2.41	173	0.021
	8.96	2.66	229	0.023
	9.7	2.90	264	0.025
	10.7	3.56	333	0.028

CO_2 density values were confirmed using the NIST data base (NIST, 1997). Day et al. (1996), Tsivintzelis et al. (2004), and Li et al. (2003) performed experiments on alcohol-treated CO_2 at pressure and temperature similar to those of our study. They showed that alcohol-treated CO_2 density is 1.03 times that of pure CO_2. This magnitude of change is similar to what is shown in Table 2.

2.2 Experimental setup and measurement of IFT

2.2.1 Experimental setup

Fig. 1(a) shows a schematic of the experimental setup, consisting of a HPHT visualization cell having two sapphire windows on opposite sides and a metal needle having a 1.52 mm diameter at the bottom. An accumulator was used to inject alcohol-treated CO_2. A metering valve was used to inject pure CO_2 and alcohol-treated CO_2 into the cell. The HPHT cell, accumulator, and injection lines for pure CO_2 and alcohol-treated CO_2 were heated to 70 °C using heating tape. An insulating tape was wrapped around the hot surfaces. A high-resolution camera was placed horizontally to capture images of pendant drop, capillary rise, and oil swelling. To obtain high-quality photos, a light source was placed on the opposite side of the cell. IFT measurements were made at 70 °C, with pressure ranging from 6.2 to 12.4 MPa.

Prior to each experimental run, the visualization cell and oil supply lines were cleaned with ethanol and water, and dried by flushing nitrogen gas to remove contamination. The pure CO_2 and alcohol-treated CO_2 lines were cleaned by blowing nitrogen gas. Capillary tubes used for the capillary rise method were cleaned with water and then dried by blowing nitrogen gas.

After preparation of the experimental fluids, IFT measurements were made using two methods, as described in subsections 2.2.2 and 2.2.3.

2.2.2 Pendant drop

For a given experimental run using the pendant drop technique, the cell was filled with oil and set to the desired temperature (70 °C). Then the cell was pressurized using pure or alcohol-treated CO_2. After the pressure stabilized, a drop of pure or alcohol-treated CO_2 was introduced through the gauge needle. Once the well-shaped drop was formed, the drop image was captured on camera. We allowed only 30-60 seconds for a well-shaped drop to remain in oil before capturing the image. This short waiting period ensured that the drop would not reach vapor-liquid equilibrium with oil. As in a realistic scenario, the high velocity of CO_2 makes it highly unlikely for CO_2 and oil to reach equilibrium near the injection well (Green and Willhite, 1998; Al-Wahaibi and Al-Hadrami, 2011; Moradi et al., 2014). The drop's shape was analyzed using ImageJ software.

Then, the IFT (γ) between the oil and gas phases (in mN/m) was calculated based on the empirical formula given

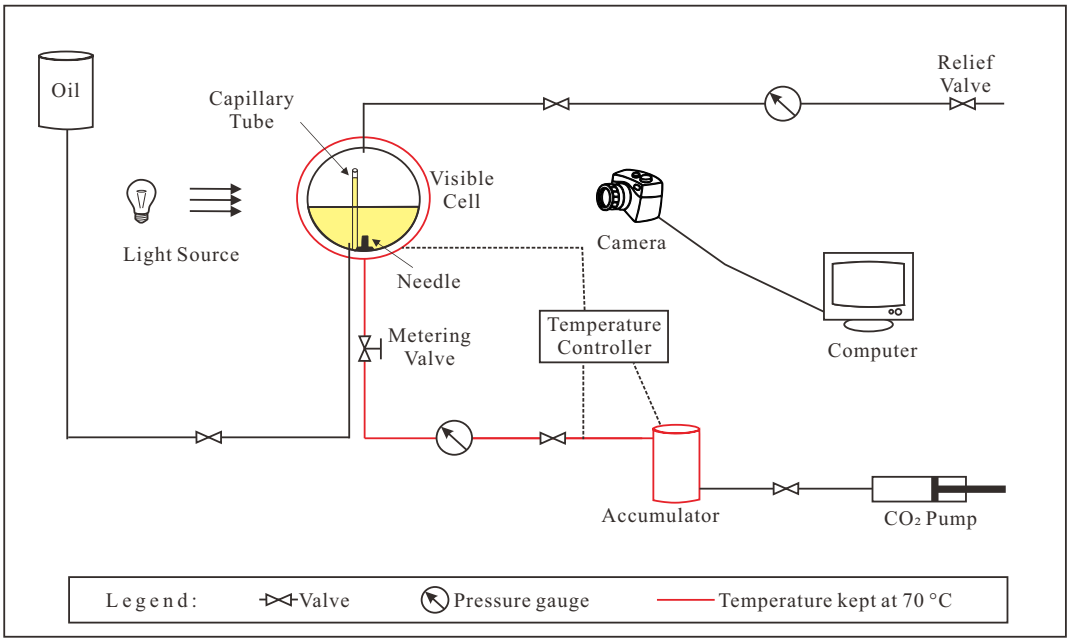

(a)

(b)

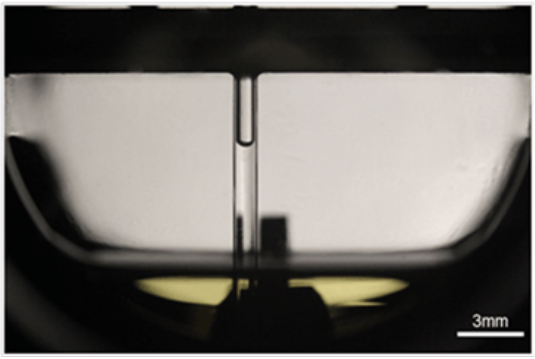

(c)

Fig. 1. (a) Schematic of experimental setup, (b) pendant drop in HPHT cell, and (c) capillary rise of oil in HPHT cell.

by Andreas et al. (2002):

$$\gamma = \frac{\Delta\rho g D_e^2}{H} \tag{1}$$

where $\Delta\rho$ is the difference in the fluids' densities in g/cc, g is the gravitational constant in cm/sec^2, D_e is the equatorial diameter of the droplet in cm, and H is a shape-correction factor that depends on the ratio between the droplet diameter measured horizontally (D_s) and D_e. The value of H can be obtained from tables provided by Andreas et al. (2002). Because the pendant drop tends to be small and flat for IFT at or below 1 mN/m, pendant drop method is best used when IFT exceeds 1 mN/m (Guo and Schechter, 1997).

2.2.3 Capillary rise and oil swelling

To measure IFT using capillary rise, an HPHT cell was partially filled with oil, and a capillary tube having a 0.3 mm internal radius was inserted into the cell. Then, pure CO_2 or alcohol-treated CO_2 was injected into the cell to achieve the desired pressure. An image of the capillary rise was then taken (Fig. 1(c)).

If the capillary rise was too small to be measured, this indicated that the pressure was just below MMP. The captured image was analyzed using ImageJ software, and the IFT (γ) between the oil and gas phases (in mN/m) was calculated by the following equation (Ayirala and Rao, 2011):

$$\gamma = \frac{rh\Delta\rho g}{2\cos\theta} \tag{2}$$

where r is the capillary tube internal radius in cm, h is the capillary rise in cm, and θ is the equilibrium contact angle in degrees. θ was measured directly from images of the contact point of the fluids' interface with capillary tubes. All of our experimental runs had a θ value of $33^\circ \pm 0.5$.

The capillary rise method can accurately measure IFT between oil and gas phases as low as 0.04 mN/m (Ayirala and Rao, 2006; Sequeira et al., 2008; Saini and Rao, 2010). Density values used in Eq. (2) assumed the composition of fluids to be same as reported in section 2.1. However,

Table 3. Experimental runs.

Experiment ID	Number of trials	Oil	Injection fluid	Pressure range (MPa)	Experimental technique	
					Capillary rise	Pendant drop
1	3		Pure CO_2	7.6-11.1	✓	
2	2	C_6-C_{10} mixture	Methanol-treated CO_2	7.0-10.7	✓	
3	1		Ethanol-treated CO_2	7.5-10.9	✓	
4	4		Pure CO_2	7.3-12.4	✓	✓
5	1	Pure C_{10}	Methanol-treated CO_2	6.3-12.5	✓	
6	3		Ethanol-treated CO_2	6.8-11.6	✓	✓

during the experiment, mass transfer caused some of ethanol or methanol to condense from the CO_2 phase into the oil phase. This mass transfer causes change in the density of oil and modified CO_2. We used a CMG simulator to estimate the variation in densities at various equilibration times, and these variations were used in the IFT calculations presented in supplementary information (Appendix C). The error lay within 0.01 to 0.24 mN/m for pure C_{10}, and 0.002 to 0.012 mN/m for the C_6-C_{10} mixture. However, as pressure approached MMP, the error attributed to density difference was at least one order of magnitude smaller than the IFT-difference reported in Section 3.3.

The capillary rise images were also used to geometrically calculate oil swelling. The swelling factor (η_{sw}) was calculated by the following equation (Emera and Sarma, 2007):

$$\eta_{sw} = \frac{V}{V_{in}} \tag{3}$$

where V_{in} is the original oil volume at room pressure and experimental temperature. V is the oil volume at experimental pressure and temperature. Detailed calculations to estimate V_{in} and V by analyzing the captured image are provided in supplementary information (Appendix A).

2.3 Experimental runs

Table 3 lists the experimental runs, each of which involved the capillary rise technique. Experimental runs 4 and 6 were also performed by the pendant drop method. The conditions of some experimental runs were repeated for reproducibility, the results of which are summarized in supplementary information (Appendix B).

2.4 Slim tube simulation

All of the experimental runs specified in Table 3 were also modeled using a 1D compositional slim tube simulated model in CMG-GEM, which was another means to determine IFT. The model consisted of a 320×1×1 grid. To model flow, an injection well was placed in grid cell, and a production well was placed in grid cell. Table 4 presents the parameters used in the simulation, which were adopted from Kamali et al. (2015). Initially, the model was fully saturated with oil. Then, it was injected with pure CO_2 or alcohol-treated CO_2. Liquid and gas relative permeability values were equal to the respective phase saturation. Two types of oil were used: a C_6-C_{10} mixture, and pure C_{10}. The Peng-Robinson equation of state (CMG-WinProp, 2018) was used for identification of liquid and vapor phase. IFT was calculated by using following equation (Reid et al., 1977).

Table 4. Properties of slim tube simulation model.

Parameter	Value
Model dimensions (number of cells)	320×1×1
Grid block length in X-direction (ft)	0.1875
Grid block length in Y-direction (ft)	0.025
Grid block length in Z-direction (ft)	0.025
Porosity (%)	30
Permeability (mD)	1000
Relative permeability	Phase saturation
Well index	1000
Reservoir temperature (°C)	70

$$\sigma^{1/4} = p_{ar}(\rho_L - \rho_V) \tag{4}$$

where σ is the IFT in dyne/cm between phases vapor and liquid, and p_{ar} is the parachor. For a hydrocarbon component i, the parachor can be defined as

$$p_{ari} = \grave{E} \times CN_i \tag{5}$$

where $\grave{E} = 40$ for $CN_i \leq 12$, and $\grave{E} = 40.3$ for $CN_i > 12$, and CN_i is the carbon number of the component i.

All simulations were run at 70 °C and various pressures (7.0-12.5 MPa). For each combination of injection fluid and oil (Table 3), a graph of simulated oil recovery at 1.2 PVI was plotted against simulated pressure. MMP was deemed the pressure at the deflection point in the curve (Li et al., 2015).

3. Results and discussion

3.1 Experimental validation

Fig. 2 compares IFT measurement using the pendant drop and capillary rise techniques. For IFT values greater than 1 mN/m, both methods are in close agreement.

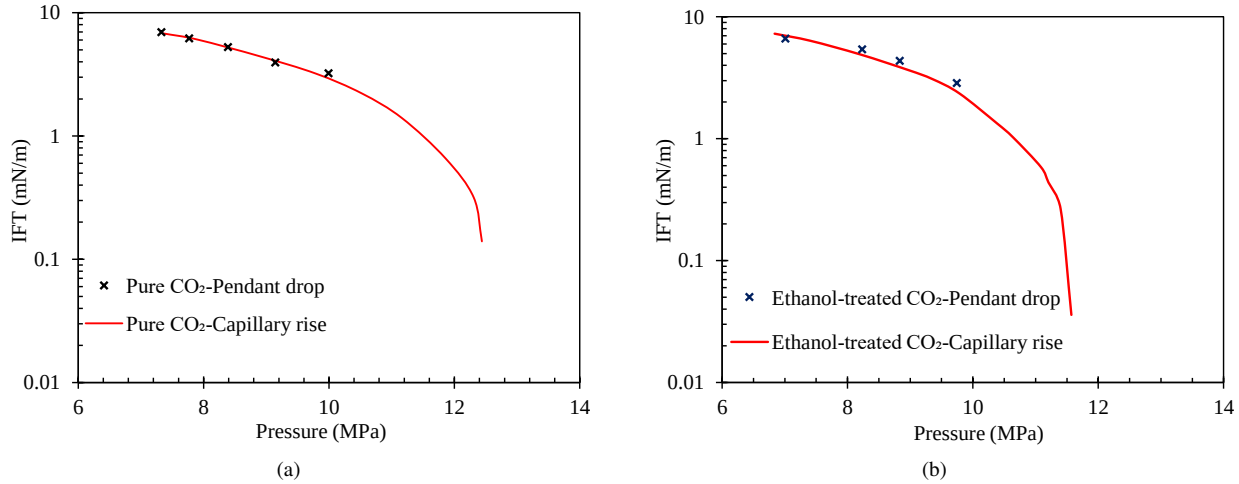

Fig. 2. IFT measurement using the pendant drop and capillary rise techniques for (a) the pure CO_2-oil system, and (b) the ethanol-treated CO_2-oil system, both involving pure C_{10}.

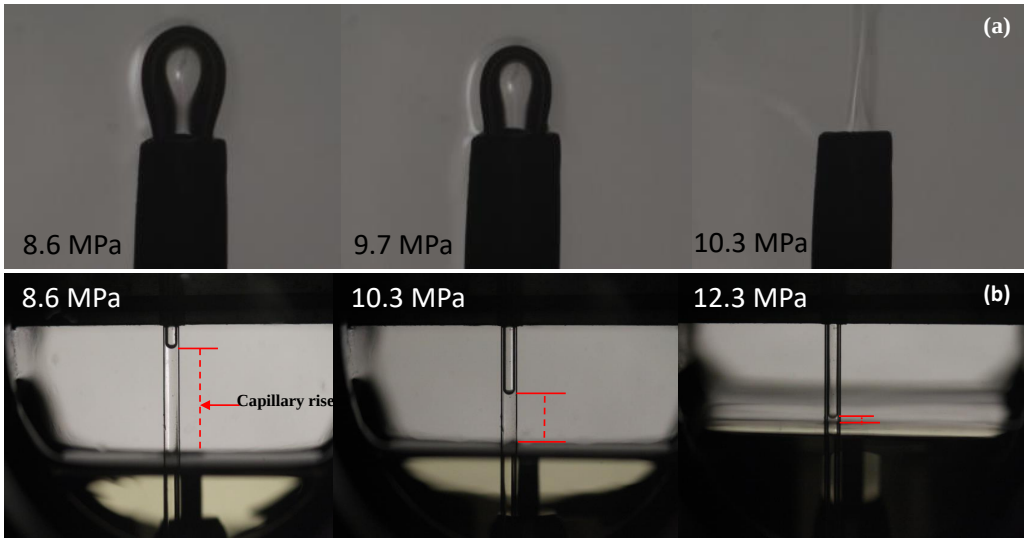

Fig. 3. Measurement of IFT for pure CO_2 and pure C_{10} systems at various pressures and 70 °C using (a) pendant drop, and (b) capillary rise images.

Fig. 3 shows pendant drop and capillary rise images for pure CO_2 and pure C_{10} at various pressures. In Fig. 3(a), the gas bubble at 8.6 MPa appears to be sharp. However, with increasing pressure, IFT between injected gas and oil reduces, making the gas bubble small and flat, as shown at 9.7 MPa. This makes analysis of the image problematic. However, as shown in Fig. 3(b), the capillary rise technique is able to measure the lower IFT values at higher pressures.

We also determined IFT through slim tube simulations for pure CO_2 and pure C_{10}, and ethanol-treated CO_2 and pure C_{10}. Fig. 4 shows that these IFT values were nearly identical to those obtained by the capillary rise technique.

Based on the experiments, standard deviation of measured IFT values was calculated as depicted by the error bars in Fig. 5. The standard deviations lie within 0.01 to 0.30 mN/m. For pure C_{10}, it reduced from 0.23 mN/m at 9.6 MPa to 0.08 mN/m at 12 MPa using pure CO_2, and from 0.23 mN/m at 8.7 MPa to 0.2 mN/m at 11.0 MPa using ethanol-treated CO_2 (Figs. 5(a) and 5(b)). For the C_6-C_{10} mixture, it reduced from 0.11 mN/m at 9.7 MPa to 0.05 mN/m at 10.9 MPa using pure CO_2 (Fig. 5(c)), and from 0.29 mN/m at 9.0 MPa to 0.01 mN/m at 10.9 MPa using methanol-treated CO_2 (Fig. 5(d)).

3.2 Miscibility determination using VIT, slim tube, and capillary rise

Fig. 6 depicts the experimental IFT data from Fig. 2, but with a linear scale along the vertical axis. At pressures insufficient to force IFT below 1 mN/m, IFT was found to decrease linearly because the fluids are immiscible and have minimum mass transfer (Thomas et al., 1994). However, at pressures sufficient to force IFT below 1 mN/m, the IFT decrease became less pronounced because more mass transfer occurs (Orr, 2007).

To determine MMP, VIT (linear extrapolation of IFT data) would have been unsuitable (Orr and Jessen, 2007). Orr and Jessen (2007) noted that VIT does not consider velocity-

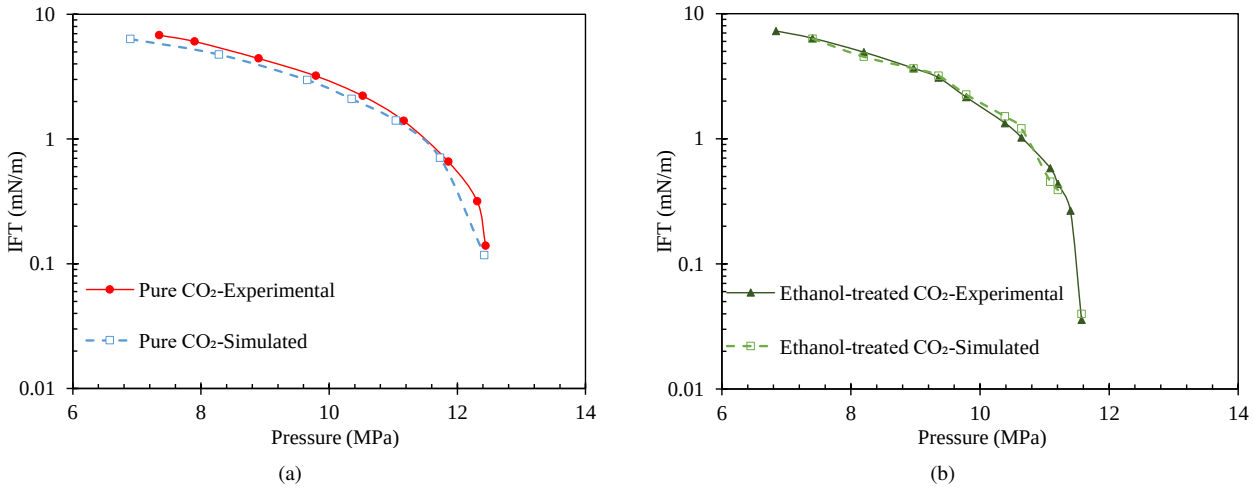

Fig. 4. Comparison of IFT values obtained for pure C_{10} by experiment (capillary rise technique) and by simulation (slim tube) for the (a) pure CO_2-oil system, and (b) ethanol-treated CO_2-oil system.

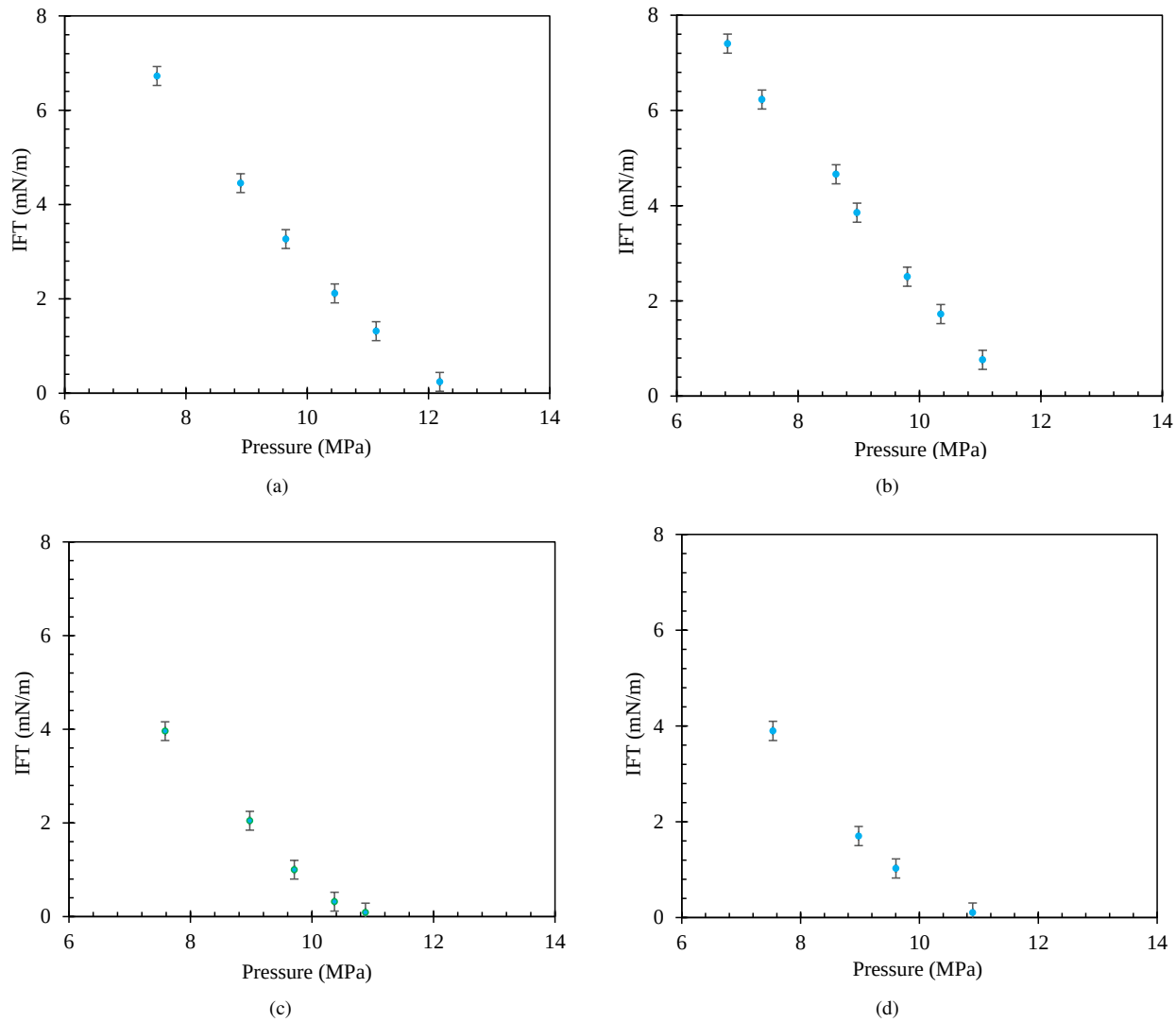

Fig. 5. Error bars for reproducible experimental runs using (a) pure CO_2 and pure C_{10} (based on four experimental runs), (b) ethanol-treated CO_2 and pure C_{10} (based on three experimental runs), (c) pure CO_2 and the C_6-C_{10} mixture (based on four experimental runs), and (d) methanol-treated CO_2 and the C_6-C_{10} mixture (based on two experimental runs).

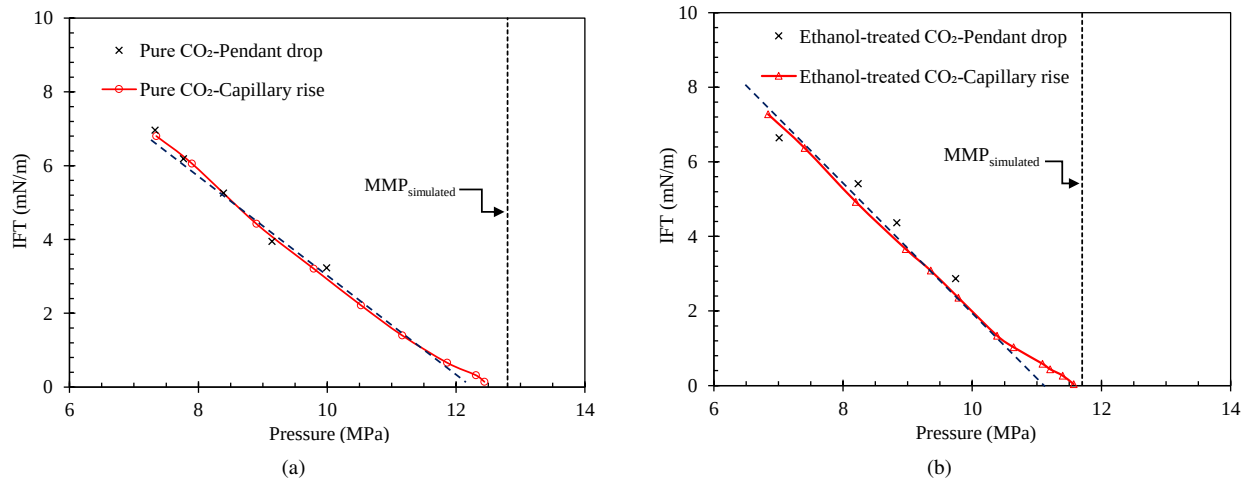

Fig. 6. Linear depiction of graphs reported in Fig. 2 for IFT using pure C_{10} with (a) pure CO_2, and (b) ethanol-treated CO_2. The vertical dashed line indicates MMP obtained by slim tube simulation. The intersection of the slanted dashed line with the x-axis depicts the MMP that would have been implied by VIT.

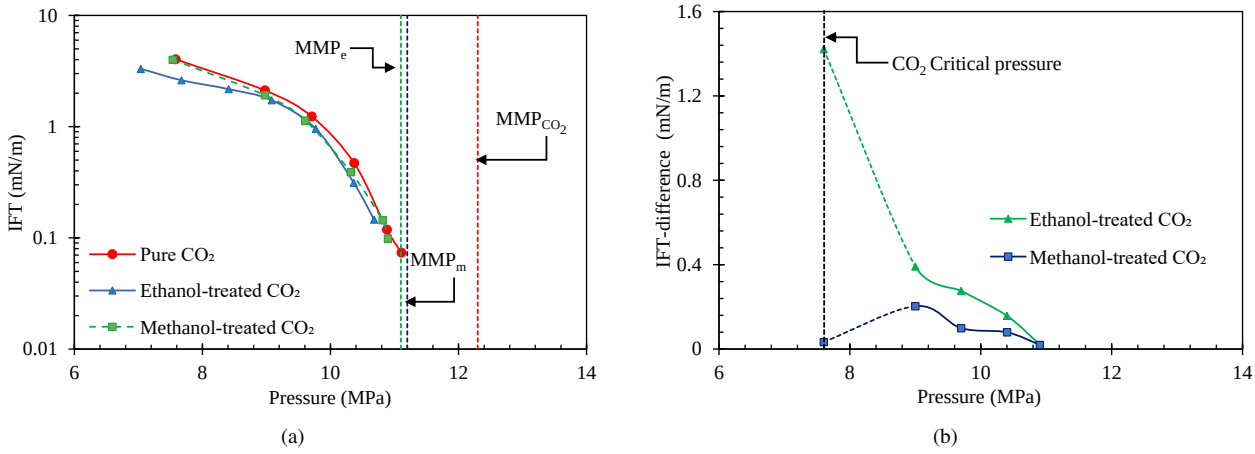

Fig. 7. Capillary rise-obtained IFT data for each injection fluid and the C_6-C_{10} mixture: (a) IFT versus pressure, with the vertical dashed lines depicting slim tube-derived MMP values, and (b) IFT-difference, with the vertical dashed line depicting the critical pressure.

dependent mass transfer between oil and the injected fluids. Therefore, the present study used slim tube simulations to estimate MMP. Fig. 6 shows that the simulated MMP was close to the pressure at which IFT inferred from capillary-rise approached zero and was much further from the pressure obtained using VIT. For pure CO_2, the lowest value of IFT was measured at 12.4 MPa, which was 0.4 MPa lower than the simulated MMP. For ethanol-treated CO_2, the lowest value of IFT was measured at 11.6 MPa, which is 0.1 MPa lower than the simulated MMP. Therefore, the capillary rise technique can be used to measure IFT under near-miscibility.

3.3 Effect of alcohol-treated CO_2 on IFT

Fig. 7(a) plots the IFT for the injection of various fluids into the C_6-C_{10} mixture. For both pure CO_2 and alcohol-treated CO_2, IFT was found to decrease as pressure increases. However, alcohol-treated CO_2 yielded consistently lower IFT than did pure CO_2 at the given pressure, which can be explained by intermolecular forces (Hrnčič et al., 2014; Rudyk et al., 2014; Kravanja et al., 2018a, 2018b).

With increasing pressure, distance between CO_2 molecules decreased, which increased the density of pure CO_2 and intermolecular forces in pure CO_2. These effects were less pronounced in oil, due to its being only slightly compressible. Therefore, with increasing pressure, the difference in density and intermolecular forces between pure CO_2 and oil reduces. This improves pure CO_2 solubility in oil, which leads to lower IFT (Yang et al., 2012).

In alcohol-treated CO_2, both CO_2 and oil molecules attach to alcohol due to strong hydrogen bonding and the hydroxyl group (Li et al., 2003; Moradi et al., 2014). Therefore, two types of interaction are involved with alcohol-treated CO_2: interaction of alcohol molecules with CO_2 molecules, and interaction of alcohol molecules with the CO_2/oil interface (Zhang et al., 2020). These interactions allow CO_2 molecules to enter the oil easily and further decrease the intermolecular forces in the oil (Yang et al., 2019). This improves solubility and density of CO_2 and brings about a lower IFT than when alcohol is not used (Zhang et al., 2020a).

To further analyze the impact of alcohol-treated CO_2 on

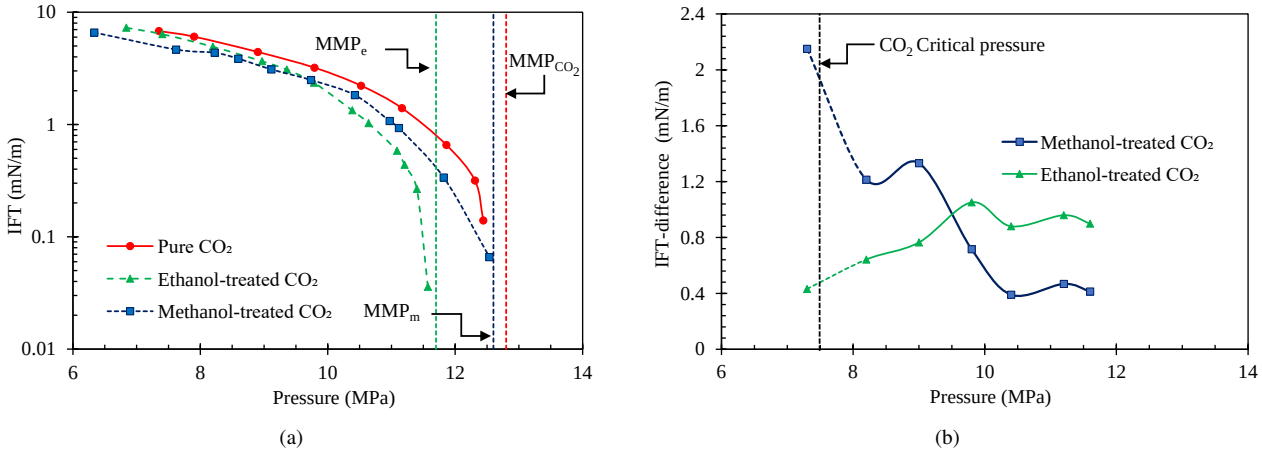

Fig. 8. Capillary rise-obtained IFT data for each injection fluid and pure C_{10}: (a) IFT versus pressure, with the vertical dashed lines depicting slim tube-derived MMP values, and (b) IFT-difference, with the vertical dashed line depicting the critical pressure.

IFT, Fig. 7(b) depicts the IFT-difference, which is defined as the IFT between pure CO_2 and oil, minus the IFT between alcohol-treated CO_2 and oil at the given pressure. A higher IFT-difference implies greater miscibility. The IFT difference was considerably higher than the standard deviation of measured IFT. Hence, the IFT difference showed the impact of alcohol in reducing IFT. For methanol-treated CO_2, IFT-difference varied from 0.02 to 0.2 mN/m; whereas for ethanol-treated CO_2, IFT-difference varied from 0.02 to 1.42 mN/m. IFT reduction was more pronounced using ethanol-treated CO_2 because longer-chain alcohols can extract heavier components of hydrocarbons more readily than can shorter-chain alcohols (Rudyk et al., 2013; Almobarak et al., 2021).

The trend in IFT-difference values below CO_2 critical pressure (7.6 MPa) appeared to differ from those measured at higher pressure (Fig. 7(b)). We measured only one data point at subcritical pressure. As the trend change from subcritical to supercritical region is unknown, we have joined the first two points using a dotted line. Being that CO_2 is supercritical under reservoir conditions, the following discussion focuses on IFT-difference above critical pressure. For both methanol-treated CO_2 and ethanol-treated CO_2, IFT-difference decreased with increasing pressure. The decrease in both curves above the critical pressure confirms Moradi et al. (2014) and Shang et al. (2018).

As the pressure increase approaches near-miscibility, IFT-difference decreases. Under near-miscibility, IFT between pure CO_2 and oil approaches zero (Thomas et al., 1994). Therefore, the significant reduction in IFT brought about by the addition of alcohol yields an IFT-difference near zero.

These patterns can be explained as follows. At lower pressures (below 9.7 MPa), pure CO_2 is immiscible with oil. Due to the presence of alcohol in CO_2, more mass transfer occurs, which leads to a higher IFT-difference. But at higher pressures, pure CO_2 starts approaching MMP, resulting in a lower IFT-difference. Once pure CO_2 reaches MMP, IFT-difference becomes zero.

Fig. 8(a) plots IFT for the injection of various fluids into pure C_{10}. As was the case for the C_6-C_{10} mixture, alcohol-treated CO_2 yielded consistently lower IFT than did pure CO_2 at the given pressure. Fig. 8(b) depicts the IFT-difference for these injection fluids into pure C_{10}. The IFT difference was considerably higher than the standard deviation of measured IFT. Hence, the IFT difference shows the impact of alcohol in reducing IFT. For methanol-treated CO_2, IFT-difference varied from 0.4 to 2.2 mN/m; whereas for ethanol-treated CO_2, IFT-difference varied from 0.4 to 1.1 mN/m.

Above critical CO_2 pressure (7.6 MPa), for both methanol-treated CO_2 and ethanol-treated CO_2, IFT-difference peaked and then decreased as pressure increased further (Fig. 8(b)). However, IFT-difference became relatively stable beyond 11 MPa as the fluid started to approach near-miscibility. These results confirm Luo et al. (2018) and Yang et al. (2019).

For methanol-treated CO_2, IFT-difference peaked at 1.33 mN/m and then decreased to 0.4 mN/m; whereas for ethanol-treated CO_2, IFT-difference peaked at 1.05 mN/m and then decreased to 0.9 mN/m. The initial increase in IFT-difference was due to the enhanced mass transfer that causes a sharp decrease in IFT between alcohol-treated CO_2 and oil. But as the pressure increased beyond a threshold, a sharp decline in IFT also occurred between pure CO_2 and oil, thereby decreasing IFT-difference until it approached zero near MMP.

Fig. 9 shows IFT results determined through slim tube simulations for different injection fluids using C_6-C_{10} mixture and pure CO_2. These simulated results are identical to experimental observations. Alcohol-treated CO_2 yielded consistently lower IFT than did pure CO_2 at the given pressure.

The different trends in IFT-difference observed for the C_6-C_{10} mixture and pure C_{10} can be attributed to the type of oil. In the C_6-C_{10} mixture, C_6, being an intermediate hydrocarbon, vaporizes into the injected CO_2; whereas C_{10}, being a heavier hydrocarbon, allows CO_2 to be condensed. Therefore, both vaporization and condensation drive mechanisms occur in the C_6-C_{10} mixture; whereas in pure C_{10}, only the condensation drive mechanism occurs.

Our IFT-difference trend matches the literature. The IFT reduction observed in Moradi et al. (2014) had a greater order of magnitude than did our IFT-difference, but only because

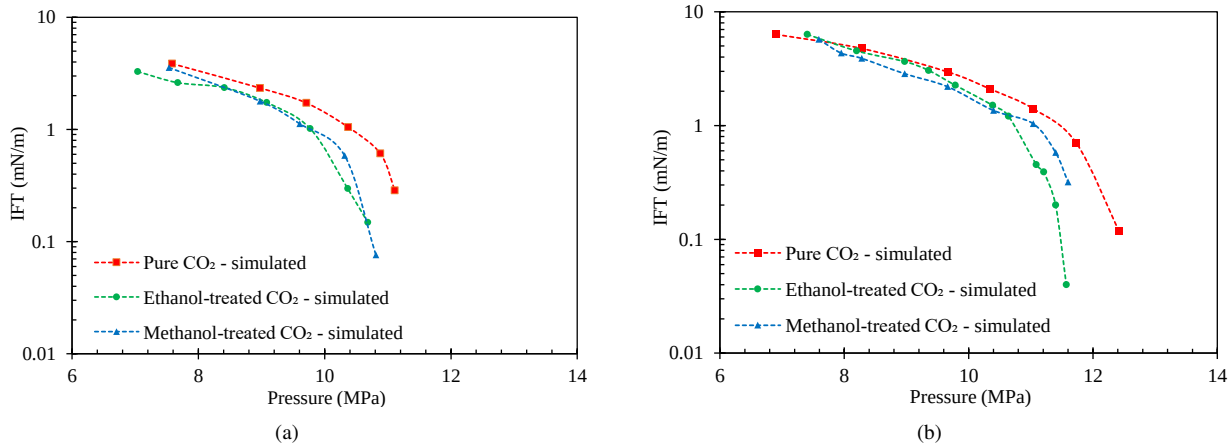

Fig. 9. Simulation obtained IFT data for each injection fluid using (a) C_6-C_{10} mixture and (b) pure C_{10}.

Table 5. Summary of MMP reduction of studied system.

Oil	Additive in CO_2	MMP for pure CO_2 and oil (MPa)	MMP for alcohol-treated CO_2 and oil (MPa)	Reduction in MMP for the given oil (MPa)
C_6-C_{10} mixture	Methanol	12.3	11.2	1.1
	Ethanol		11.1	1.2
Pure C_{10}	Methanol	12.8	12.6	0.2
	Ethanol		11.7	1.1

they used heavier alcohols such as $C_{12}H_{25}OH$ and employed it to modify oil rather than CO_2. Using a heavier alcohol to modify CO_2 is ill-advised because of its low solubility in CO_2. Our IFT-difference values are similar to Shang et al. (2018) and Luo et al. (2018) except that these two studies reported the minimum IFT-difference to be 0.9 and 1.1 mN/m respectively, which are greater than what we reported (0.02). This is because we were able to measure IFT-difference at pressures closer to MMP, at which IFT-difference is nearly zero.

Being that the reduction in IFT also indicates improved miscibility, ethanol- and methanol-treated CO_2 yielded lower MMP than did pure CO_2 (Figs. 7(a) and 8(a)). The MMP values are summarized in Table 5. Similar MMP reduction was observed for ethanol- and methanol-treated CO_2 with the C_6-C_{10} mixture and for ethanol-treated CO_2 with pure C_{10}. However, methanol-treated CO_2 with pure C_{10} reduced MMP by only 0.2 MPa. Greater MMP reduction associated with ethanol-treated CO_2 shows its greater ability to achieve miscibility than that of methanol-treated CO_2.

3.4 Effect of alcohol-treated CO_2 on oil swelling

Selected images taken for visual observation of oil swelling are presented in Fig. 10 for the C_6-C_{10} mixture and Fig. 11 for pure C_{10}. Fig. 10 shows the oil swelling at pressures 0 MPa, 9.0 MPa, and 10.9 MPa for pure CO_2 and the C_6-C_{10} mixture. Comparing the three sub-figures of Fig. 10 makes evident that for the C_6-C_{10} mixture, ethanol-treated CO_2 brought about the most oil swelling.

Fig. 11 shows the oil swelling from injecting the various fluids into pure C_{10}. Ethanol-treated CO_2 and methanol-treated CO_2 exhibited comparable oil swelling, which exceeded that for pure CO_2.

Figs. 12(a) and 12(b) plot the oil swelling for the injection of various fluids into the C_6-C_{10} mixture and pure C_{10}. They show that for each combination of injection fluid and oil, oil swelling occurred as the pressure increased. As discussed in section 3.3, CO_2 solubility increases with pressure, which causes the oil to swell (Yang et al., 2012). However, in alcohol-treated CO_2, the inherent polarity of alcohol causes more CO_2 solubility in oil (Li et al., 2003). Therefore, oil swelling is greater with alcohol-treated CO_2. To further analyze the impact of alcohol-treated CO_2 on oil swelling, Figs. 12(c) and 12(d) depict the swelling-difference, which is defined as swelling of oil injected with alcohol-treated CO_2, minus the swelling of oil injected with pure CO_2 at the given pressure. For the C_6-C_{10} mixture (Fig. 12(c)), swelling-difference for methanol-treated CO_2 varied from 0.14 to 0.43; whereas swelling-difference for ethanol-treated CO_2 varied from 0.18 to 0.36. The increase in oil swelling is higher for ethanol-treated CO_2 than for methanol-treated CO_2. This is consistent with the results in section 3.3 that showed IFT-difference and MMP reduction to be greater for ethanol-treated CO_2 than for methanol-treated CO_2.

For pure C_{10} (Fig. 12(d)), swelling-difference for ethanol-treated CO_2 varied from 0.08 to 0.35; whereas swelling-difference for methanol-treated CO_2 varied from 0.06 to 0.22.

Further, a sharp increase in oil swelling was observed with alcohol-treated CO_2 for the C_6-C_{10} mixture after 10.6 MPa and for pure C_{10} after 11.6 MPa. This occurred when pure

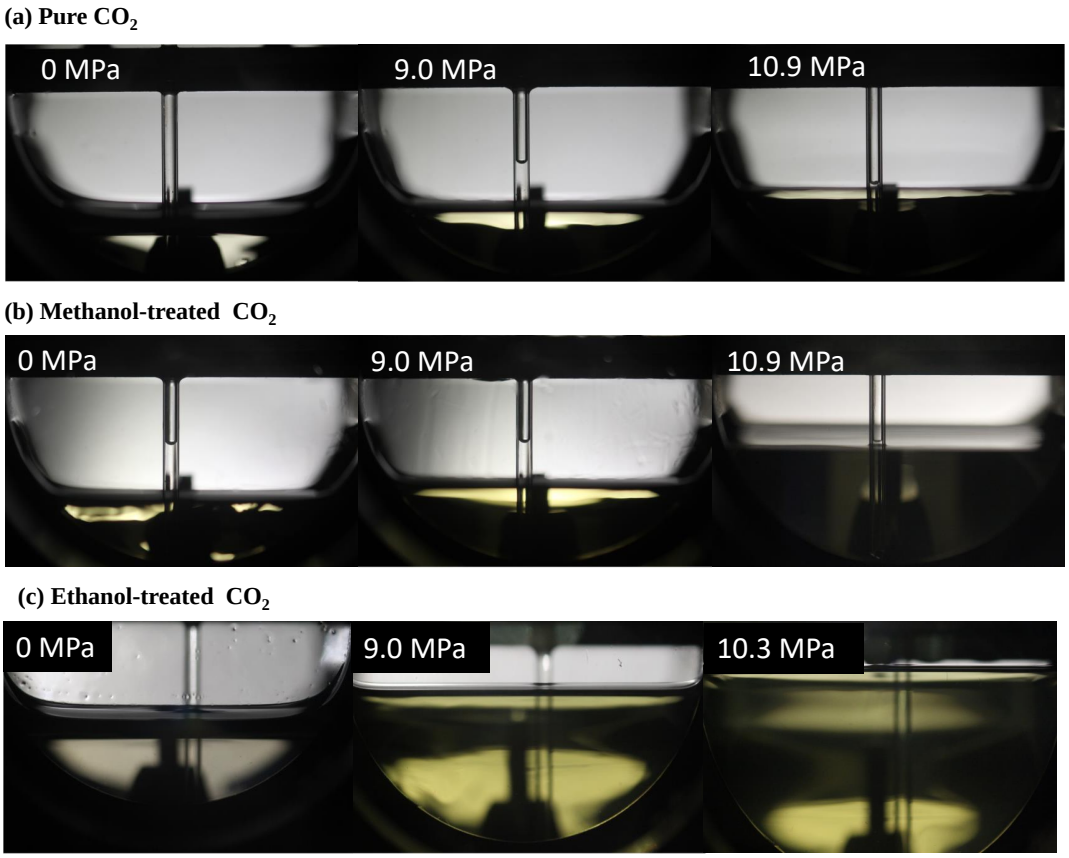

Fig. 10. Oil swelling of the C_6-C_{10} mixture observed from injecting (a) pure CO_2, (b) methanol-treated CO_2, and (c) ethanol-treated CO_2.

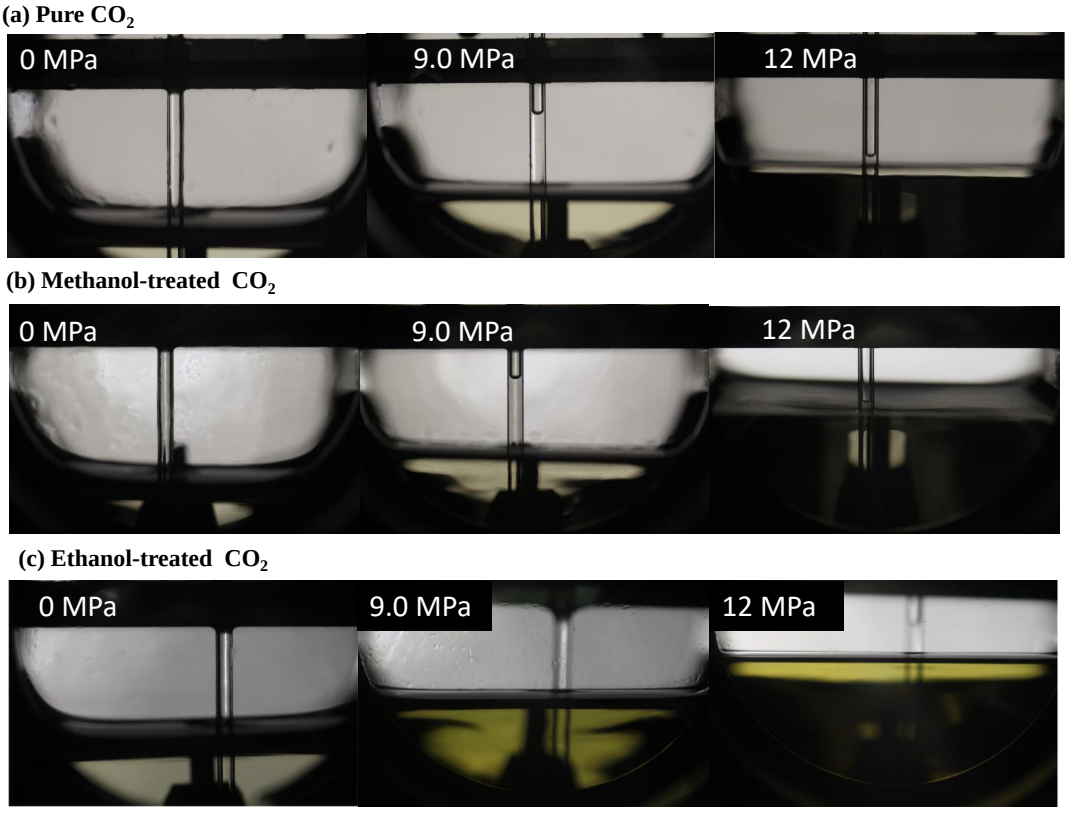

Fig. 11. Oil swelling of pure C_{10} observed from injecting (a) pure CO_2, (b) methanol-treated CO_2, and (c) ethanol-treated CO_2.

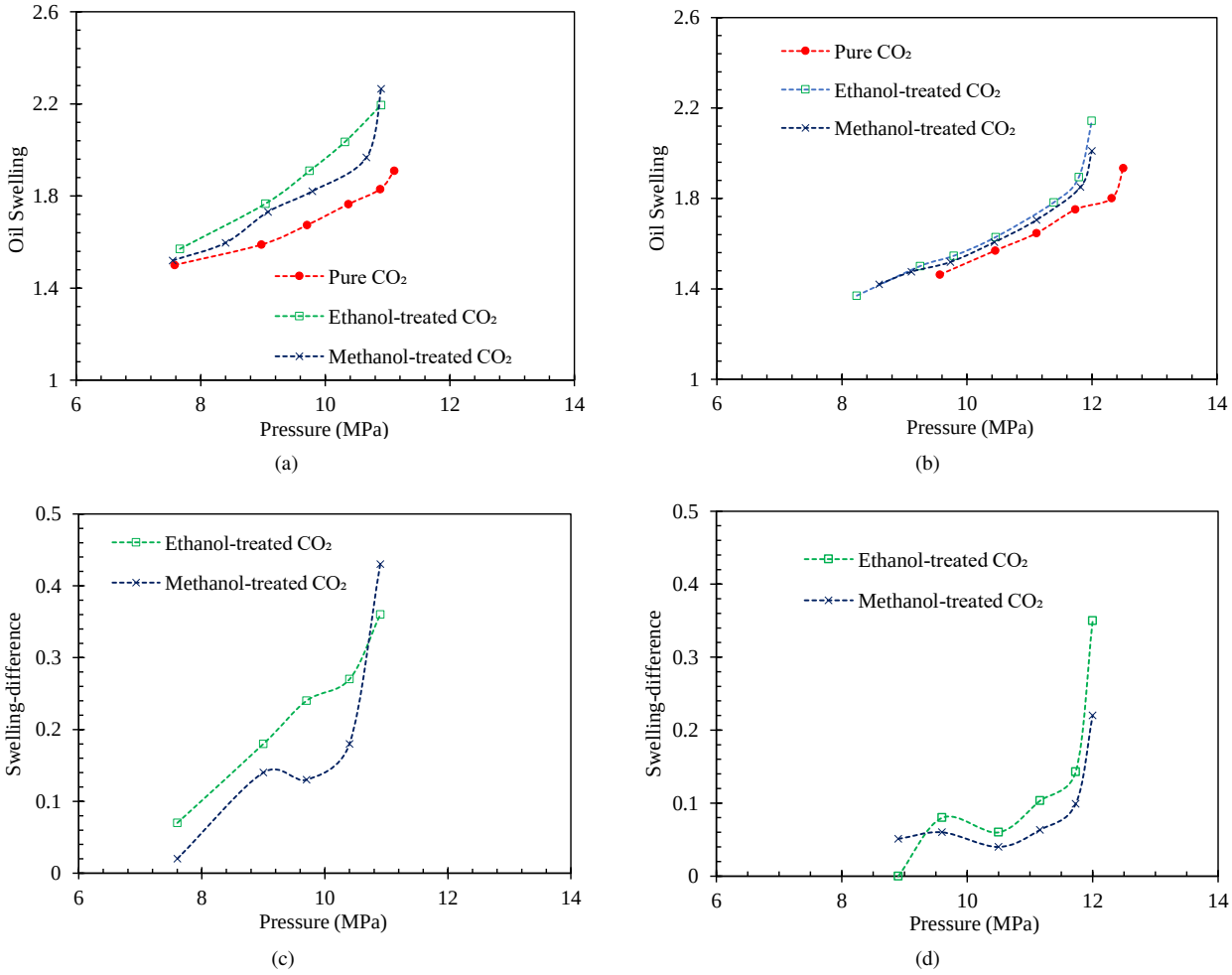

Fig. 12. Oil swelling versus pressure for each injection fluid (a) the C_6-C_{10} mixture, (b) pure C_{10}, and swelling-difference for each alcohol-treated injection fluid, (c) the C_6-C_{10} mixture, and (d) pure C_{10}.

CO_2 IFT reached near-miscibility (Figs. 7(a) and 8(a)). The presence of alcohol in CO_2 resulted in more mass transfer and therefore rapid oil swelling.

4. Conclusions

This paper presented an experimental study of the extent to which treating CO_2 with ethanol-treated alcohol or methanol-treated alcohol prior to injecting it in an oil reservoir affects miscibility. The oils were a C_6-C_{10} mixture and pure C_{10}. Interfacial tension (IFT) and oil swelling were measured in each experimental run. Slim tube simulations were used to corroborate the experimentally determined IFT and minimum miscibility pressure (MMP). The following conclusions are drawn:

1) IFT as low as 0.04 mN/m was studied using the capillary rise technique. The reliability of the IFT results was verified through the pendant drop technique and through reproducibility.
2) Both the experiment and simulation showed that alcohol-treated CO_2 injection brought about lower IFT and MMP than did pure CO_2 injection. For the C_6-C_{10} mixture, the IFT reduction was 0.02 to 0.2 mN/m with methanol-treated CO_2 and 0.02 to 1.42 mN/m with ethanol-treated CO_2. For pure C_{10}, the IFT reduction was 0.4 to 1.2 mN/m with methanol-treated CO_2 and 0.4 to 1.1 mN/m with ethanol-treated CO_2.
3) Our simulation indicated that the presence of methanol in CO_2 reduced MMP by 1.1 MPa for the C_6-C_{10} mixture and 0.2 MPa for pure C_{10}. The presence of ethanol in CO_2 was found to reduce MMP by 1.2 MPa for the C_6-C_{10} mixture and 1.1 MPa for pure C_{10}.
4) Alcohol-treated CO_2 resulted in significantly more oil swelling than did pure CO_2. Methanol-treated CO_2 yielded 0.14 to 0.43 greater swelling of the C_6-C_{10} mixture and 0.06 to 0.22 greater swelling of pure C_{10} than that achieved by pure CO_2. Ethanol-treated CO_2 yielded 0.18 to 0.36 greater swelling of the C_6-C_{10} mixture and 0.08 to 0.35 greater swelling of pure C_{10} than that achieved by pure CO_2.
5) Ethanol-treated CO_2 was found more effective at reducing IFT and MMP and at increasing oil swelling than was methanol-treated CO_2 or pure CO_2.
6) IFT and swelling results suggest that alcohol-treated CO_2 yields better miscibility with oil compared to pure CO_2.

This study utilized only straight chain alcohols to modify CO_2. More experiments should be performed to investigate other additives. Hexane (C_6) and decane (C_{10}) used in this study have some impurity (5%), which might affect accuracy of experimental results. Further, we used slim tube simulations to determine MMP between CO_2 and oil and alcohol-treated CO_2 and oil. Literature suggests that such determination of MMP is qualitative only and for accurate estimation of MMP, slim tube experiments should be performed. However, the studied method depicts qualitative effect of alcohol-treated CO_2 and CO_2 on MMP.

Acknowledgement

The authors would like to thank CMG Ltd for allowing us access to the GEM and Winprop simulators. The authors thank David H. Levin for editing the manuscript. Saira would like to acknowledge the Pakistan Higher Education Commission (HEC) for sponsoring her PhD studies.

Conflict of interest

The authors declare no competing interest.

References

Ahmad, W., Vakili-Nezhaad, G., Al-Bemani, A. S., et al. Uniqueness, repeatability analysis and comparative evaluation of experimentally determined MMPs. Journal of Petroleum Science and Engineering, 2016, 147: 218-227.

Ahmed, T. Minimum miscibility pressure from eos. Paper SPE 137404 Presented at Canadian Unconventional Resources and International Petrolrum Conference, Calgary, Alberta, Canada, 19-21 October, 2000.

Aji, A. Q. M., Awang, M., Yusup, S. Fatty acid methyl ester from rubber seed oil as additives in reducing the minimum miscibility pressure of CO_2 and crude oil. Journal of Applied Sciences, 2016, 16(11): 542-548.

Al Hinai, N. M., Myers, M. B., Dehghani, A. M., et al. Effects of oligomers dissolved in CO_2 or associated gas on ift and miscibility pressure with a gas-light crude oil system. Journal of Petroleum Science and Engineering, 2019, 181: 106210.

Almobarak, M., Wu, Z., Myers, M. B., et al. Chemical-assisted minimum miscibility pressure reduction between oil and methane. Journal of Petroleum Science and Engineering, 2021, 196: 108094.

Al-Wahaibi, Y. M., Al-Hadrami, A. K. The influence of high permeability lenses on immiscible, first- and multi-contact miscible gas injection. Journal of Petroleum Science and Engineering, 2011, 77(3-4): 313-325.

Amooie, M. A., Soltanian, M. R., Moortgat, J. Hydrothermodynamic mixing of fluids across phases in porous media. Geophysical Research Letters, 2017, 44(8): 3624-3634.

Andreas, J. M., Hauser, E. A., Tucker, W. B. Boundary tension by pendant drops1. The Journal of Physical Chemistry, 2002, 42(8): 1001-1019.

Ayirala, S. C., Rao, D. N. Comparative evaluation of a new mmp determination technique. Paper SPE 99606 Presented at SPE/DOE Symposium on Improved Oil Recovery, Tulsa, Oklahoma, USA, 22-26 April, 2006.

Ayirala, S. C., Rao, D. N., Casteel, J. Comparison of minimum miscibility pressures determined from gas-oil interfacial tension measurements with equation of state calculations. Paper SPE 84187 Presented at SPE Annual Technical Conference and Exhibition, Denver, Colorado, 5-8 October, 2003.

Bagci, A. Immiscible CO_2 flooding through horizontal wells. Energy Sources, Part A, 2007, 29(1): 85-95.

Bedrikovetsky, P. Wag displacements of oil-condensates accounting for hydrocarbon ganglia. Transport in Porous Media, 2003, 52(2): 229-266.

Bezanehtak, K., Combes, G. B., Dehghani, F., et al. Vapor-liquid equilibrium for binary systems of carbon dioxide + methanol, hydrogen + methanol, and hydrogen + carbon dioxide at high pressures. Journal of Chemical & Engineering Data, 2002, 47(2): 161-168.

Bikkina, P., Wan, J., Kim, Y., et al. Influence of wettability and permeability heterogeneity on miscible CO_2 flooding efficiency. Fuel, 2016, 166: 219-226.

Chen, H. I., Chang, H. Y., Chen, P. H. High-pressure phase equilibria of carbon dioxide + 1-butanol, and carbon dioxide + water + 1-butanol systems. Journal of Chemical & Engineering Data, 2002, 47(4): 776-780.

Chen, H. I., Chen, P. H., Chang, H. Y. High-pressure vapor-liquid equilibria for CO_2 + 2-butanol, CO_2 + isobutanol, and CO_2 + tert-butanol systems. Journal of Chemical & Engineering Data, 2003, 48(6): 1407-1412.

Chen, S., Gong, Z., Li, X., et al. Pore structure and heterogeneity of shale gas reservoirs and its effect on gas storage capacity in the qiongzhusi formation. Geoscience Frontiers, 2021, 12(6): 101244.

Choubineh, A., Helalizadeh, A., Wood, D. A. Estimation of minimum miscibility pressure of varied gas compositions and reservoir crude oil over a wide range of conditions using an artificial neural network model. Advances in Geo-Energy Research, 2019, 3(1): 52-66.

CMG-WinProp. CMG-Winprop PVT. Calgary, Canada CMG, 2018.

Dai, Z., Middleton, R., Viswanathan, H., et al. An integrated framework for optimizing CO_2 sequestration and enhanced oil recovery. Environmental Science & Technology Letters, 2014, 1(1): 49-54.

Day, C. Y., Chang, C. J., Chen, C. Y. Phase equilibrium of ethanol + CO_2 and acetone + CO_2 at elevated pressures. Journal of Chemical & Engineering Data, 1996, 41(4): 839-843.

Dong, P., Liao, X., Chen, Z., et al. An improved method for predicting CO_2 minimum miscibility pressure based on artificial neural network. Advances in Geo-Energy Research, 2019, 3(4): 355-364.

Emera, M. K., Sarma, H. K. Prediction of CO_2 solubility in oil and the effects on the oil physical properties. Energy Sources, Part A, 2007, 29(13): 1233-1242.

Ershadnia, R., Wallace, C. D., Soltanian, M. R. CO_2 geological sequestration in heterogeneous binary media: Effects of geological and operational conditions. Advances in Geo-Energy Research, 2020, 4(4): 392-405.

Green, D. W., Willhite, G. P. Enhanced Oil Recovery. Texas, USA, Henry L. Doherty Memorial Fund of AIME, Society of Petroleum Engineers, 1998.

Gu, Y., Zhang, S., She, Y. Effects of polymers as direct CO_2 thickeners on the mutual interactions between a light crude oil and CO_2. Journal of Polymer Research, 2013, 20(2): 61.

Guo, B., Schechter, D. S. A simple and accurate method for determining low ift from pendant drop measurements. Paper SPE 37216 Presented at International Symposium on Oilfield Chemistry, Houston, Texas, 18-21 Febeuary, 1997.

Gupta, R. B., Shim, J. J. Solubility in Supercritical Carbon Dioxide. Boca Raton, USA, CRC Press, 2006.

Hrnčič, M. K., Markočič, E., Trupej, N., et al. Investigation of thermodynamic properties of the binary system polyethylene glycol/CO_2 using new methods. The Journal of Supercritical Fluids, 2014, 87: 50-58.

Iglauer, S., Al-Yaseri, A. Improving basalt wettability to de-risk CO_2 geo-storage in basaltic formations. Advances in Geo-Energy Research, 2021, 5(3): 347-350.

Joung, S. N., Yoo, C. W., Shin, H. Y., et al. Measurements and correlation of high-pressure vle of binary CO_2-alcohol systems (methanol, ethanol, 2-methoxyethanol and 2-ethoxyethanol). Fluid Phase Equilibria, 2001, 185(1-2): 219-230.

Kamali, F., Hussain, F., Cinar, Y. A laboratory and numerical-simulation study of co-optimizing CO_2 storage and CO_2 enhanced oil recovery. SPE Journal, 2015, 20(6): 1227-1237.

Kathel, P., Mohanty, K. K. EOR in tight oil reservoirs through wettability alteration. Paper SPE 166281 Presented at SPE Annual Technical Conference and Exhibition, New Orleans, Louisiana, USA, 30 September-2 October, 2013.

Kravanja, G., Knez, Ž., Hrnčič, M. K. Density, interfacial tension, and viscosity of polyethylene glycol 6000 and supercritical CO_2. The Journal of Supercritical Fluids, 2018a, 139: 72-79.

Kravanja, G., Knez, Ž., Hrnčič, M. K. The effect of argon contamination on interfacial tension, diffusion coefficients and storage capacity in carbon sequestration processes. International Journal of Greenhouse Gas Control, 2018b, 71: 142-154.

Kuang, N., Yang, S., Yuan, Z., et al. Study on oil and gas amphiphilic surfactants promoting the miscibility of CO_2 and crude oil. ACS Omega, 2021, 6(41): 27170-27182.

Lake, L.W. Enhanced oil recovery. United States, 1989.

Li, F., Yang, S., Chen, H., et al. An improved method to study CO_2-oil relative permeability under miscible conditions. Journal of Petroleum Exploration Production Technology, 2015, 5(1): 45-53.

Li, J., Rodrigues, M., Matos, H. A., et al. Vle of carbon dioxide/ethanol/water: Applications to volume expansion evaluation and water removal efficiency. Industrial & Engineering Chemistry Research, 2005, 44(17): 6751-6759.

Li, P., Yi, L., Liu, X., et al. Screening and simulation of offshore CO_2-EOR and storage: A case study for the HZ21-1 oilfield in the Pearl River Mouth Basin, Northern South China Sea. International Journal of Greenhouse Gas Control, 2019, 86: 66-81.

Li, Q., Wang, Y., Wang, X., et al. An application of thickener to increase viscosity of liquid CO_2 and the assessment of the reservoir geological damage and CO_2 utilization. Energy Sources, Part A, 2019, 41(3): 368-377.

Li, Q., Zhang, Z., Zhong, C., et al. Solubility of solid solutes in supercritical carbon dioxide with and without cosolvents. Fluid Phase Equilibria, 2003, 207(1-2): 183-192.

Liu, B., Fu, X., Li, Z. Impacts of CO_2-brine-rock interaction on sealing efficiency of sand caprock: A case study of shihezi formation in ordos basin. Advances in Geo-Energy Research, 2018, 2(4): 380-392.

Luo, H., Zhang, Y., Fan, W., et al. Effects of non-ionic surfactant (C_iPO_j) on the interfacial tension behavior between CO_2 and crude oil. Energy & Fuels, 2018, 32(6): 6708-6712.

Moradi, B., Awang, M., Bashir, A., et al. Effects of alcohols on interfacial tension between carbon dioxide and crude oil at elevated pressures and temperature. Journal of Petroleum Science and Engineering, 2014, 121: 103-109.

NIST Chemistry Webbook. Washington, D.C. National Institute of Standards and Technology, 1997.

Orr, F. M. Theory of Gas Injection Processes. Copenhagen, Denmark, Tie-Line Publications, 2007.

Orr, F. M., Jessen, K. An analysis of the vanishing interfacial tension technique for determination of minimum miscibility pressure. Fluid Phase Equilibria, 2007, 255(2): 99-109.

Rao, D. N. A new technique of vanishing interfacial tension for miscibility determination. Fluid Phase Equilibria, 1997, 139(1): 311-324.

Reid, R. C., Sherwood, T. K., Prausnitz, J. M. The properties of gases and liquids. United States, 1977.

Ren, J., Wang, Y., Feng, D., et al. CO_2 migration and distribution in multiscale-heterogeneous deep saline aquifers. Advances in Geo-Energy Research, 2021, 5(3): 333-346.

Renner, R. Tracking the dirty byproducts of a world trying to stay clean. American Association for the Advancement of Science, 2004, 306(5703): 1887.

Rommerskirchen, R., Bilgili, H., Fischer, J., et al. Impact of miscibility enhancing additives on the flooding scheme in CO_2 EOR processes. Paper SPE 190288 Presented at SPE Improved Oil Recovery Conference, Tulsa, Oklahoma, USA, 14-18 April, 2018.

Rommerskirchen, R., Nijssen, P., Bilgili, H., et al. Reducing the miscibility pressure in gas injection oil recovery processes. Paper SPE 183389 Presented at Abu Dhabi International Petroleum Exhibition & Conference, Abu Dhabi, UAE, 7-10 November, 2016.

Rudyk, S., Hussain, S., Spirov, P. Supercritical extraction of crude oil by methanol-and ethanol-modified carbon

dioxide. The Journal of Supercritical Fluids, 2013, 78: 63-69.

Rudyk, S., Spirov, P., Hussain, S. Effect of co-solvents on SC-CO_2 extraction of crude oil by consistency test. The Journal of Supercritical Fluids, 2014, 91: 15-23.

Saini, D., Rao, D. N. Experimental determination of minimum miscibility pressure (mmp) by gas/oil ift measurements for a gas injection EOR project. Paper SPE 132389 Presented at the SPE Western Regional Meeting, Anaheim, California, USA, 27-29 May, 2010.

Saira, Ajoma, E., Le-Hussain, F. A laboratory investigation of the effect of ethanol-treated carbon dioxide injection on oil recovery and carbon dioxide storage. SPE Journal, 2021, 26(5): 3119-3135.

Saira, Janna, F., Le-Hussain, F. Effectiveness of modified CO_2 injection at improving oil recovery and CO_2 storage-review and simulations. Energy Reports, 2020, 6: 1922-1941.

Schneider, C. A., Rasband, W. S., Eliceiri, K. W. NIH Image to ImageJ: 25 years of image analysis. Nature Methods, 2012, 9(7): 671-675.

Sequeira, D. S., Ayirala, S. C., Rao, D. N. Reservoir condition measurements of compositional effects on gas-oil interfacial tension and miscibility. Paper SPE 113333 Presented at SPE Symposium on improved Oil Recovery, Tulsa, Oklahoma, USA, 20-23 April, 2008.

Shang, Q., Xia, S., Cui, G., et al. Experiment and correlation of the equilibrium interfacial tension for paraffin + CO_2 modified with ethanol. The Journal of Chemical Thermodynamics, 2018, 116: 206-212.

Thomas, F. B., Holowach, N., Zhou, X., et al. Miscible or near-miscible gas injection, which is better? Paper SPE 27811 Presented at SPE/DOE improved Oil Recovery Symposium, Tulsa, Oklahoma, 17-20 April, 1994.

Tsivintzelis, I., Missopolinou, D., Kalogiannis, K., et al. Phase compositions and saturated densities for the binary systems of carbon dioxide with ethanol and dichloromethane. Fluid Phase Equilibria, 2004, 224(1): 89-96.

Tunio, S. Q., Tunio, A. H., Ghirano, N. A., et al. Comparison of different enhanced oil recovery techniques for better oil productivity. International Journal of Applied Science and Technology, 2011, 1(5): 143-153.

Yang, Z., Li, M., Peng, B., et al. Dispersion property of CO_2 in oil. 1. Volume expansion of CO_2 + alkane at near critical and supercritical condition of CO_2. Journal of Chemical & Engineering Data, 2012, 57(3): 882-889.

Yang, Z., Wu, W., Dong, Z., et al. Reducing the minimum miscibility pressure of CO_2 and crude oil using alcohols. Colloids and Surfaces A: Physicochemical and Engineering Aspects, 2019, 568: 105-112.

Zhang, C., Xi, L., Wu, P., et al. A novel system for reducing CO_2-crude oil minimum miscibility pressure with CO_2-soluble surfactants. Fuel, 2020a, 281: 118690.

Zhang, L., Wang, Y., Miao, X., et al. Geochemistry in geologic CO_2 utilization and storage: A brief review. Advances in Geo-Energy Research, 2019, 3(3): 304-313.

Zhang, X., Ge, J., Kamali, F., et al. Wettability of sandstone rocks and their mineral components during CO_2 injection in aquifers: Implications for fines migration. Journal of Natural Gas Science and Engineering, 2020b, 73: 103050.